Available online at www.sciencedirect.com
ScienceDirect
Catalysis Today 125 (2007) 229–238
CATALYSIS TODAY
www.elsevier.com/locate/cattod

Hydrotreating of light cycle oil using WNi catalysts containing hydrothermally and chemically treated zeolite Y

Lianhui Ding [a], Ying Zheng [a,*], Zisheng Zhang [b], Zbigniew Ring [c], Jinwen Chen [c]

[a] *Department of Chemical Engineering, University of New Brunswick, 15 Dineen Drive, PO Box 4400, Fredericton, NB E3B 5A3, Canada*
[b] *Department of Chemical Engineering, University of Ottawa, Ottawa, Ont. K1N 6N5, Canada*
[c] *National Centre for Upgrading Technology, 1 Oil Patch Drive, Suite A202, Devon, Alta. T9G 1A8, Canada*

Available online 27 February 2007

Abstract

One W–Ni catalyst supported on hydrothermally treated zeolite Y and two W–Ni catalysts supported on chemically treated zeolite Y were prepared. The catalysts were characterized by NH_3-TPD, pyridine-IR, TEM, BET, and XPS. Their performance of hydrodesulfurization, hydrodenitrogenation, and hydrodearomatization were compared using light cycle oil (LCO) as the feed. The results showed that the hydrothermal treatment promotes HDS activity whereas the chemical approach favours the HDA activity. The HDN activity of the three catalysts was similar. Addition of zeolite Y with high proportion of Brønsted acidity in the catalysts helps to enhance the hydrodearomatization activity.

Keywords: Hydrotreating; LCO; Catalysts; Zeolite Y; Hydrothermal treatment; Chemical treatment

1. Introduction

Extensive studies have revealed that the addition of acidic components into the traditional alumina-supported hydrotreating catalysts can greatly enhance their hydrodesulfurization (HDS) and hydrodearomatization (HDA) activities [1–3]. Among the acidic components, zeolite Y is the most studied and widely commercially applied [4,5]. Though the acidic zeolite helps to enhance HDS activity of the catalysts, it will also increase deactivation of the catalyst and overcracking of diesel fraction. The overcracking of the diesel fractions not only lowers the yield of diesel fuel, but also increases hydrogen consumption. To improve the HDS activity of refractory sulfur species and avoid a rapid deactivation and overcracking of the diesel distillate, the surface acidity of zeolite should be properly modified.

It has been demonstrated that the total acidity and the acid strength distribution of zeolite catalysts are primarily controlled by the framework silicon-to-aluminum ratio [6,7]. The framework silicon-to-aluminum ratio can be properly modified through dealumination using the following two methods: (1) hydrothermal treatment [8,9]; (2) chemical treatment in which the framework aluminum is normally replaced by silicon atoms from $SiCl_4$ in gaseous phase [10] or from $(NH_4)_2SiF_6$ (AHFS) in liquid phase [11,12]. The distinguished discrepancies between hydrothermal and chemical treatment mainly are: (1) the dealuminated zeolite obtained under hydrothermal conditions contains extra-framework aluminum (EFAL) species; while the chemical treatment is able to produce a perfect lattice structure with negligible amounts of extra-framework aluminum [12,13]; (2) the secondary mesopores can be produced after hydrothermal treatment [14,15], while nearly no secondary mesopores are formed after the chemical treatment; (3) hydrothermally treated zeolite possesses both Brønsted and Lewis acidic sites, and sometimes strong acidic sites may be created [16,17]. The predominant acidic sites in chemically treated zeolites are Brønsted sites.

The difference in catalytic properties reflects the structural and chemical variations between the zeolites treated by the two methods. The comparison of the cracking activities of the small molecules (heptane) and large molecules (vacuum gasoil) [12] indicated that the activity for *n*-heptane cracking is approximately the same for a steam and an AHFS dealuminated sample, while the gasoil cracking activity of AHFS dealuminated sample is lower than that of a steam treated one. In FCC process [18], the AHFS dealuminated Y zeolites appeared

* Corresponding author. Tel.: +1 506 447 3329; fax: +1 506 453 3591.
E-mail address: yzheng@unb.ca (Y. Zheng).

0920-5861/$ – see front matter
doi:10.1016/j.cattod.2007.01.054

more stable during steaming in regenerator section of FCC unit than the hydrothermally treated zeolites. The AHFS dealuminated Y zeolites retained higher crystallinity, and contained smaller amounts of amorphous acid debris, and thus exhibited higher activity retention and gasoline selectivity.

Almost all the comparisons between chemical and hydrothermal treated zeolites Y [12,18–21] were made in the catalytic cracking reaction in which only zeolite Y was used as a cracking component, and no hydrogenation metals, W(Mo) or Ni(Co), were added. Meanwhile, the reactions occurred in the absence of hydrogen. Although numerous studies have been conducted under hydrotreating conditions and with gasoil or heavy oils as feedstocks [22–24], almost all the studies were based on hydrothermally treated zeolite Y (USY), and no comparison was made between chemical and hydrothermal treated zeolite.

In the area of hydrotreating of light cycle oil (LCO), little work has been done concerning the hydrogenation performance of the hydrothermally and chemically treated zeolite Y. The main purpose of this work is to investigate the difference between chemically and hydrothermally treated zeolites in hydrotreating LCO.

2. Experimental

2.1. Preparation of zeolites

Chemically treated zeolite Y (CTY) was synthesized using the method described in Ref. [13]. In a flask, 95 g of NH_4NaY (Zeolyst CBV-300) was stirred with a 1.0 M ammonium acetate solution at 348 K, and then 200 ml of a 0.8 M AHFS solution were dropwisely added to the flask. The sample was stirred at 368 K for 24 h, followed by thoroughly washing with boiling water, and then dried at 383 K overnight, which was designated as CTY. The dried CTY sample was further hydrothermally treated at 823 K, 0.1 MPa for 1 h in an autoclave reactor, which was designated as HCTY.

The hydrothermally treated zeolite Y (HTY) was prepared by treating NH_4NaY (Zeolyst CBV-300) under ''self-steaming'' conditions in an autoclave reactor at 823 K and 0.1 MPa for 1 h, followed by being twice subjected to ammonia exchanges with 1.0 M NH_4Cl aqueous solution at 363–368 K, and then dried at 383 K overnight.

2.2. Catalyst preparation

The supports were prepared by mixing the zeolites, large-pore alumina (22 wt% or 37 wt%, Sasol PURALOX TH100/150, the pore volume: 0.96 ml/g, the surface area: 201.6 m^2/g), and a binder (20 wt%, partially acid-peptized alumina, SASOL, CAPAPAL B), extruded to form the cylindrical extrudate, dried at 383 K overnight, and then calcined in the air at 823 K for 4 h. The NiW catalysts were prepared by co-impregnation of the above extrudates using the incipient wetness method with an aqueous solution of the appropriate amount of nickel nitrate hexahydrate [$Ni(NO_3)_2{\cdot}6H_2O$] and ammonium metatungstate [$(NH_4)_6H_2W_{12}O_{40}$], dried at 383 K overnight, and calcinated at 773 K for 4 h. The zeolite contents in the catalysts were 28 wt% HCTY, 15 wt% HCTY, and 28 wt% HTY zeolite, which were designated as WNi/HCTY28, WNi/HCTY15, and WNi/HTY28, respectively. WO_3 and NiO in all catalysts were about 24 wt% and 6 wt%, respectively.

2.3. Catalyst characterization

2.3.1. NH_3 temperature programmed desorption (NH_3-TPD)

0.5 g of 30–40 mesh sample was loaded into a 5 ml tubular reactor, and then purged 2 h with 40 ml/min helium at 773 K (increased from ambient temperature to 773 K at 5 K/min), followed by lowering temperature to 353 K. Fifty millilitres per minute of gaseous ammonia mixed with 40 ml/min helium was charged for 30 min at 353 K, and then purge with 40 ml/min He at 373 K for 1 h. Under the 40 ml/min of helium, the temperature was raised from 373 K to 883 K at 15 K/min, and the desorbed ammonia was analyzed by MS.

2.3.2. Powder X-ray diffraction (XRD)

The crystallinity and phase purity of solid products were characterized by using Bruker AXS D8 ADVANCE (Cu Kα radiation provided by a graphite monochromator). The peak heights of six lines [(5 1 1), (4 4 0), (5 3 3), (6 4 2), (6 6 0), and (5 5 5)] were used for the calculation of the crystallinity of the zeolites considering the crystallinity of parent NH_4NaY as 100%. Using silicon as internal standard, the unit cell size a_0 was calculated from the average of at least 15 reflections of known Miller indices. The concentration of framework aluminum atoms was determined according to Breck's equation [25]:

$$N_{Al} = 115.2(a_0 - 24.191)$$

where N_{Al} is the number of aluminum atoms per unit cell. The atomic framework Si/Al ratio was derived from the calculated N_{Al}.

2.3.3. Transmission electron microscopy (TEM)

TEM was performed on a JEOL 2010 STEM, operated at 200 keV. The spectra were collected using an EDAX Genesis 4000 system. Samples were prepared by drop method. A small amount of sulfided catalyst powder was sonicated in 100% ethanol. One drop was removed with a micropipette and dropped onto a copper (or nickel) support grid. The sample was then lightly coated with carbon to reduce charging in the TEM.

2.3.4. X-ray photoelectron spectroscopy (XPS)

XPS spectra of the samples were taken in a VG Microtech MultiLab ESCA 2000 system with a CLAM4 hemispherical analyzer. The hemispherical analyzer consists of an analysis chamber for taking the XPS spectra, which was operated under a vacuum of lower than 4×10^{-10} mbar, and a fast entry air lock for sample introduction. The source was non-monochromatized Mg Kα X-rays at 1253.6 eV (15 kV, 20 mA). In order to sample a deeper depth, photoelectron detection perpendicular to the sample surface was chosen. The high resolution C 1s spectrum of the adventitious hydrocarbon (at

284.5 eV) on the sample surfaces was recorded before and after each measurement and used as a reference for charge correction. Quantitative information of surface composition was obtained from integrated peak intensities and atomic sensitivity factors using the Advantage data acquisition and processing software supplied by Thermo VG Scientific. Peak fits of all spectra were performed using the Shirley background correction and Gaussian–Lorentzian curve synthesis.

2.3.5. BET

Nitrogen adsorption measurements were performed on a Quantachrome Autosorb-1. Before adsorption, the samples were calcined at 823 K for 16 h. Powder samples of 30–40 mg were degassed in a sample preparation station under 473 K and a vacuum of 1.33×10^{-3} Pa for 15 h, and then switched to the analysis station for adsorption and desorption under a temperature of 77 K in liquid nitrogen. Surface area was calculated with the multipoint BET equation with linear region in the P/P_0 range of 0.05–0.35. Pore volume was calculated from the maximum adsorption amount of nitrogen at $P/P_0 = 0.99$.

2.3.6. Pyridine infrared (IR)

Adsorbed pyridine infrared spectra were recorded on a BIO-RAD FTS-60 Spectrometer. The samples (10 mg) were ground, mixed with KBr, and then pressed to form wafers of 1 cm in diameter, and installed on the support. The sample cell was heated to 573 K under vacuum (1.33×10^{-3} Pa) overnight, cooled to room temperature, and pyridine was then introduced into the cell and the adsorption was performed. The excess and physically adsorbed pyridine was evacuated under vacuum at room temperature overnight. Infrared spectra in the range of 1000 cm^{-1} and 4000 cm^{-1} were recorded. Total acidity of Lewis or Brønsted acid sites is obtained by integrating the corresponding band (subtracting the baseline).

The bulk silicon-to-aluminum ratios of the dealuminated samples, including framework and non-framework aluminum, were determined by chemical analysis.

2.4. Evaluation of catalyst activity

2.4.1. Nitrogen-tolerance test of HTY and HCTY

With *n*-heptane and *n*-dodecane as model compounds, nitrogen-tolerance test of HTY and HCTY was carried out in a fixed-bed reactor in a dry flow of nitrogen under the following conditions: ambient pressure, LHSV 10 h^{-1}, and reaction temperature 723 K. 0.5 g of 20–40 mesh zeolite particles were loaded. After steady cracking conversions were obtained, the feed was switched to *n*-heptane containing 1000 ppm nitrogen (pyridine) until the constant conversions were reached. Afterwards, the catalyst was purged with nitrogen for 4 h, and then the feed was switched back to pure *n*-heptane and *n*-dodecane to obtain cracking conversions.

2.4.2. LCO hydrotreating

The catalyst activity evaluation was carried out in a 1 l stirred autoclave (Autoclave Engineers Division of Snap-tite, Inc., Eze-Seal stirred reactor) with LCO. The properties of LCO were listed in Table 1. Twenty grams of catalyst was loaded in the catalyst basket in the reactor. The reactor was repeatedly vacuumed and refilled with hydrogen to replace the air in the autoclave. Five millilitres of sulfiding agent, dimethyl disulfide (DMDS), was vacuumed in the reactor. Prior to heating the reactor, the reactor was pressurized to 3.45 MPa. The catalyst was sulfided in situ at 593 K for 2 h and 633 K for another 2 h. After the sulfidation, 200 g of LCO were charged into the batch autoclave reactor through a feed charging tank amounted on the top of the reactor. The reactor was pressurized to 4.83 MPa, temperature was increased to 648 K at a rate of 3 K/min under the 1000 rpm stirring. When the temperature reached the set temperature, the hydrogen pressure was adjusted to 8.96 MPa. When the pressure drop rate was less than 1.38 kPa/min, the pressure was raised to 8.96 MPa again. The evaluation was completed when the pressure became nearly constant. The liquid product was collected, weighed, and analyzed. The nitrogen, sulfur, and aromatic were analyzed according to ASTM D4629 (syringe/inlet oxidative combustion and chemiluminescence detection, absolute experimental error was ±4 ppm), ASTM D4294 (energy-dispersive X-ray fluorescence spectrometry, absolute experimental error was ±2.5 ppm), and ASTM D6591 (high performance liquid chromatography method with refractive index detection, absolute experimental error was ±0.3 wt%), respectively. The boiling ranges of LCO and liquid products were measured with simulated distillation by gas chromatography. The liquid yield was calculated from the following equation:

$$x\ (\%) = \frac{200 - x_1}{200} \times 100$$

where x is liquid yield (%) and x_1 stands for the weight (g) of liquid product collected from reactor.

Table 1
Properties of LCO feed

Density (g/ml) (298 K)	0.9591
Nitrogen (ppmw)	495.6
Sulfur (wt%)	1.3
Saturates (wt%)	12.4
Monoaromatics (wt%)	19.0
Diaromatics (wt%)	47.0
Polyaromatics (wt%)	21.6
Distillation (K)	
0.5 wt%/10 wt%	406/487
20 wt%/30 wt%	508/527
40 wt%/50 wt%	540/555
60 wt%/70 wt%	574/591
80 wt%/90 wt%	611/635
95 wt%	650

3. Results and discussion

3.1. The textural, the acidity, and nitrogen-tolerance comparison of HTY, CTY, and HCTY zeolites

The isotherms of the starting parent NH_4NaY, hydrothermally treated zeolite Y (HTY), chemically treated zeolite Y

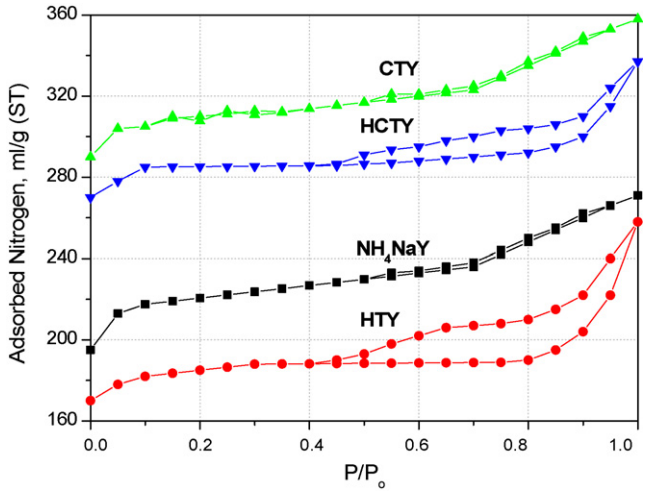

Fig. 1. Isotherms of NH_4NaY raw material, HTY, CTY, and HCTY.

(CTY), and hydrothermally treated CTY (HCTY) are illustrated in Fig. 1. The nitrogen adsorption curves of the parent NH_4NaY and CTY zeolite corresponded to type I in the Brunauer classification, which was typical for the crystalline microporous materials and characterised by a very flat adsorption–desorption isotherm with nearly no hysteresis loop. This means that the microporous character of CTY zeolite was largely retained and did not possess any appreciable mesopore volume (Table 2). After hydrothermal treatment, the hysteresis loops appeared in HTY and HCTY, clearly indicating the existence of mesoporous structures. Other main properties of the four zeolites were summarized in Table 2.

Due to either hydrothermal or chemical treatment, the pore volumes and surface areas of the zeolites are seen to decrease. After hydrothermal treatment, approximately 32% of secondary pores were created in HTY. The formation of secondary pores may result from the collapse of part of the lattice structures, which was evidenced by the very low crystallinity (85%) of HTY. In HTY and HCTY, the aluminum contents were noticeably larger than the framework aluminum concentration, indicating the presence of large amounts of extra lattice or non-framework aluminum. For CTY, along with dealumination, the silicon is able to concurrently be inserted back in the vacancies left by the removed aluminum. The dealumination process via AHFS makes CTY maintain high crystal integrity (105% crystallinity). The Si/Al ratio between the framework Si/Al ratio obtained from the unit cell size is similar to the bulk Si/Al ratio obtained by chemical analysis. This demonstrates that neither secondary pore nor non-framework aluminum were introduced to the CTY. HTY possesses a large number of both types of acid sites with a ratio of Brønsted to Lewis acid sites of 0.59. Nevertheless, in the case of CTY, the dealumination treatment led to a sample with very few Lewis sites. The Lewis acidic sites in HTY are obviously imparted by the non-framework aluminum residing in the supercages or channels. Due to the higher framework aluminum and the existence of non-framework aluminum, HTY had higher acidity than CTY.

Table 2
Properties of starting material and final zeolite products

	Raw NH_4NaY	HTY	CTY	HCTY
Na_2O (wt%)	2.8	0.07	0.08	0.08
Bulk Si/Al ratio	2.63	2.63	4.85	4.85
Framework Si/Al ratio[a]	2.43	4.31	4.84	7.37
Unit cell size	24.68	24.51	24.48	24.39
Relative crystallinity	100	85	105	102
Pore volume (ml/g)	0.42	0.40	0.40	0.37
Surface area (m^2/g)	925	783	820	743
Pore distribution (%)				
<1.7 nm	98	68	98	82
1.7–5.0 nm	2	19	2	10
5.0–15 nm	0	11	0	7.0
>15 nm	0	2.0	0	1.0
Average pore size (nm)	1.82	2.04	1.95	2.00
Pyridine-IR acidity				
Total (mmol/g)		1.37	1.19	0.81
B		0.51	1.16	0.56
L		0.86	0.03	0.25
B/L ratio		0.59	39.67	2.24

[a] From $N_{Al} = 115.2\ (a_0 - 24.191)$.

Similarly, when hydrothermally treating CTY, a considerable number of Lewis acidic sites and secondary pores were formed. However, compared with HTY, HCTY had a higher proportion of Brønsted acidic sites (B/L = 2.24), lower proportion of secondary pores (18%), and higher crystallinity (102%), probably due to the stabilization effect of framework silicon enrichment.

With more aluminum removed from lattice, framework Si/Al ratios almost linearly increased with the decrease of unit cell sizes for both hydrothermally and chemically treated zeolites, as a result of replacing trivalent Al atoms with smaller tetravalent Si atoms (1.43 Å versus 1.32 Å atomic radius).

Along with the dealumination, Na_2O content (0.08 wt%) of CTY was simultaneously reduced and reached the level of HTY which was achieved by two post ammonium exchanges. From the industrial preparation point of view, the elimination of these two ammonia exchanges not only saves energy, but also increases the product yield.

In LCO and other heavy petroleum fractions, organic nitrogen compounds coexist with sulfur compounds and aromatics. The nitrogen species, especially basic nitrogen, strongly inhibit HDS and HDA reactions, due to their strong interaction with acid sites of acidic catalysts. In order to investigate the ''nitrogen-tolerance'' performance of the HTY and HCTY, the activity recovery comparison was made before and after pyridine ''poisoned'' the HTY and HCTY. The results

Table 3
Nitrogen-tolerance of HTY and HCTY

Zeolite	HTY	HCTY
Before nitrogen poison		
n-Heptane conversion (wt%)	98.9	97.5
n-Dodecane conversion (wt%)	100	100
Activity resume after nitrogen poison		
Heptane conversion (wt%)	13.2	18.7
Dodecane conversion (wt%)	45.8	82.7

Table 4
Properties of the supports and catalysts

	WNi/HTY28	WNi/HCTY15	WNi/HCTY28
Support			
BET surface area (m^2/g)	462	377	448
Pore volume (ml/g)	0.52	0.59	0.50
Average pore size (nm)	4.46	6.30	4.44
Catalyst[a]			
BET surface area (m^2/g)	207	221	225
Pore volume (ml/g)	0.38	0.37	0.36
Average pore size (nm)	7.34	6.70	6.40
Acidity[b] (mmol/g)	0.607	0.506	0.553
Weak	0.317	0.302	0.276
Medium	0.146	0.124	0.129
Strong	0.143	0.080	0.148
Average length of WS_2 slabs[c] (nm)	22.4	17.7	31.9
Average number per WS_2 slab[c]	4.7	4.4	4.6

[a] Calcined oxidic catalyst.
[b] Obtained from NH_3-TPD.
[c] Obtained from TEM.

are summarized in Table 3. 5.5 wt% and 36.9 wt% higher activity recovery was realized by HCTY than HTY in heptane and dodecane cracking experiments, respectively, demonstrating that HCTY has higher nitrogen-tolerance ability than HTY.

3.2. Textural and acidity comparison between the supports and catalysts

Table 4 lists the main physico-chemical properties of WNi/HTY28, WNi/HCTY15, and WNi/HCTY28. In comparison to the supports, the surface areas and pore volumes of all the catalysts were drastically decreased. The surface areas decreased about 50%, and pore volumes decreased 26–37%. The pore size distributions of the three catalysts were very broad (20–300Å) and have similar pattern (Fig. 2). The average pore sizes of WNi/HTY28 and WNi/HCTY28 were greatly enlarged when W and Ni were incorporated into the corresponding supports. The increase extent of WNi/HTY28 was more pronounced.

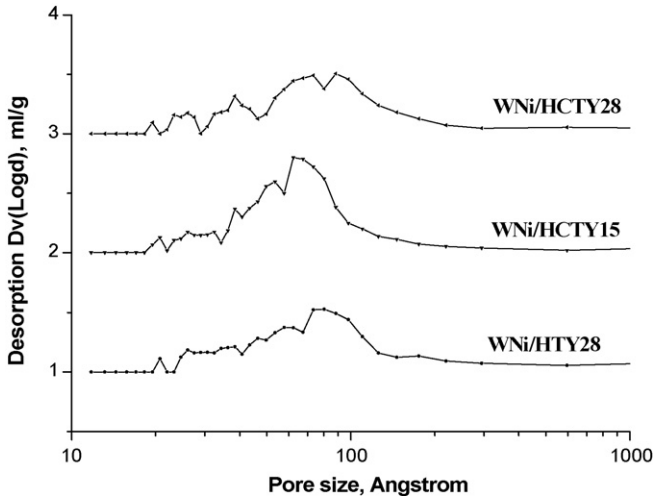

Fig. 2. Pore size distributions of WNi/HTY28, WNi/HCTY15, and WNi/HCTY28.

Fig. 3 presents the total acidity, Brønsted acidity (B), Lewis acidity (L), and B/L ratios of the supports and catalysts. For both supports and catalysts, compared with WNi/HCTY28, the total acidity of WNi/HTY28 was much higher. The incorporation of W and Ni caused the total acidity decrease. The decreasing extent for WNi/HTY28 (28%) was much less than that for WNi/HCTY28 (28%). WNi/HTY28 attained a higher proportion of Lewis acidic sites. After the addition of hydrogenation metals, more Brønsted acidic sites were preserved by WNi/HCTY28 (B/L changed from 0.42 to 0.10) than WNi/HTY28 (B/L changed from 0.81 to 0.41). When the content of the HCTY zeolite was reduced by about half (from 28% to 15%) in the catalyst, the total acidity of the support was also reduced approximately by half. However, the total acidity of the WNi/HCTY15 catalyst decreased less than that of WNi/HCTY28 and the B/L ratio was also kept at a higher level (0.27).

In order to compare the acidic strength of the three catalysts, a NH_3-TPD experiment was conducted and the results were

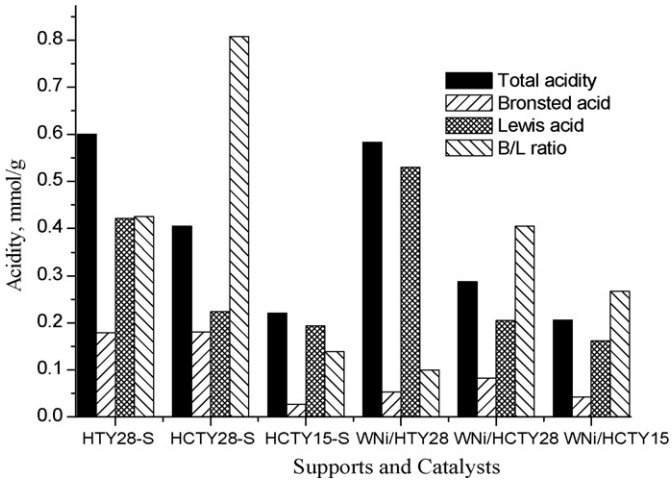

Fig. 3. Acidic types and their distributions of the supports (HTY28-S, HCTY28-S, and HCT15-S) and their corresponding WNi catalysts, obtained from pyridine-IR.

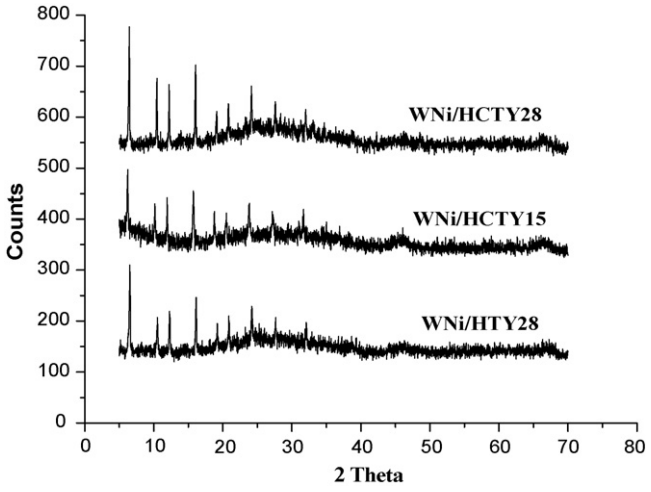

Fig. 4. XRD profiles of WNi/HTY28, WNi/HCTY15, and WNi/HCTY28.

summarized in Table 3. The weak, medium, and strong acidity were assigned to the peak areas of NH_3-TPD curves lower than 623 K, 623–773 K, higher than 773 K, respectively. Compared with WNi/HTY28, WNi/HCTY28 possessed a higher ratio of the acidic sites with strong strength. Surprisingly, WNi/HCTY15 had a much lower ratio of the strong acidic sites. In agreement with the results of pyridine-IR, the total acidity of the three catalysts decreased in the same order.

3.3. XRD of the catalysts

The XRD profiles of the catalysts in the form of oxide are shown in Fig. 4. No detectable XRD crystallines of any W or Ni species were present in the oxidic catalysts, suggesting that the tungsten and nickel oxidic species were either completely amorphous or composed of crystallites smaller than 4 nm. The WO_3 and NiO can be considered to be evenly distributed on the surface of the support. The characteristic diffraction peaks of γ-Al_2O_3 and zeolite Y (2θ 12, 16, 19, 20, and 24) appeared in all samples. The zeolite Y in WNi/HCTY had a higher crystallinity than that in WNi/HTY, mainly due to the higher crystallinity of HCTY than HTY.

3.4. XPS of the catalysts

W 4f and Ni 2p XPS spectra of three oxidic and sulfided catalysts are shown in Figs. 5 and 6, respectively. The binding energies of W, Ni, and S for oxidic and sulfided samples, surface W and Ni distribution, and S/W + Ni ratios are summarized in Table 5. The spectra of the oxidic catalysts show a doublet peak of W $4f_{5/2}$ and W $4f_{7/2}$ electrons at a binding energy (BE) position of 37.8–38.1 and 35.7–36.0 eV, respectively. These peaks are assigned to W^{6+} species, most likely W^{6+} O_3 [26]. The main peak in the Ni 2p X-ray photoelectron spectra of the oxidic samples was assigned to the spin-splitting Ni $2p_{3/2}$ (BE about 856 eV) [27]. After sulfidation, a second doublet peak appeared at about 34.7 and 32.5 eV, which are typical for tungsten with a formal charge state of 4+ as in WS_2 phase [28]. The Ni $2p_3$ XPS spectra of the sulfided catalysts

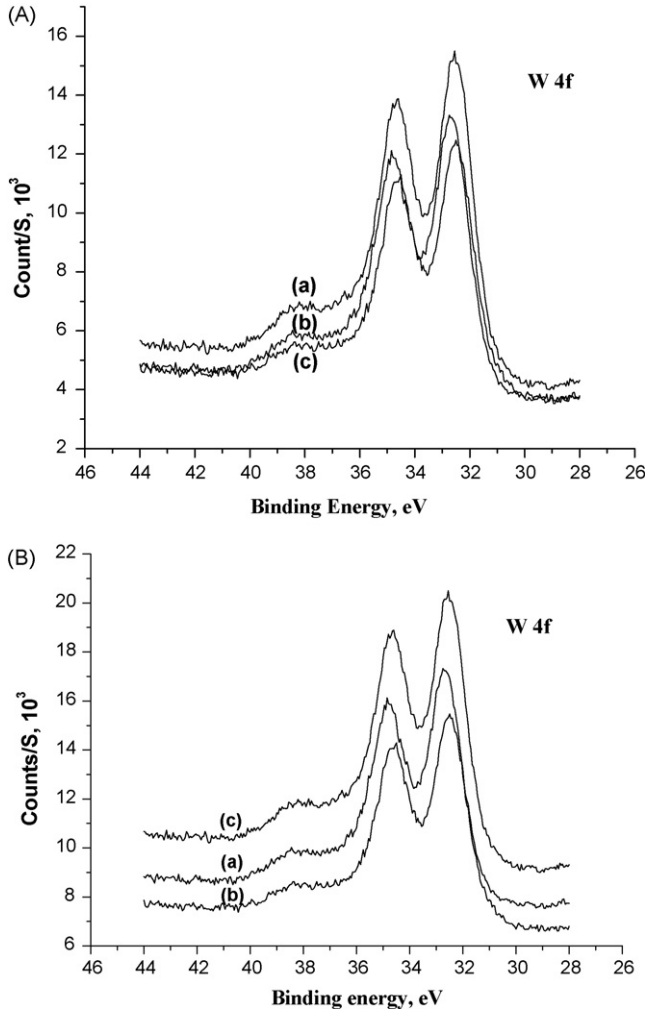

Fig. 5. XPS W 4f spectra of oxidic (A) and sulfided (B) catalysts: (a) WNi/HTY28; (b) WNi/HCTY15; (c) WNi/HCTY28.

present a relatively intense peak at about 854 eV and a second broad band overlapped partially with the first one, whose BE at around 856 eV. The shape of the Ni 2p envelope with a satellite peak clearly shows the presence of non-sulfided Ni^{2+} species in all catalysts after sulfidation. The Ni $2p_3$ peak at 856 eV is also due to the presence of the non-sulfided Ni^{2+} species [29]. The second Ni $2p_{3/2}$ peak at 853.9–854.4 eV, together with the presence of the S $2p_{3/2}$ peak at 162 eV, is associated with nickel sulfides [29]. The S 2p spectra of all the sulfided catalysts exhibit one peak at the binding energy value of 162.0 ± 0.2, which can be assigned to S^{2-} [28]. No signal was identified around BE 169 eV, indicating that no sulfate species existed [30], thus no oxidation of the catalysts occurred during the transfer of the solid from the sulfiding reactor to the XPS chamber.

For both W and Ni, in the oxidic state, the BEs of W 4f and Ni 2p core levels decreased in the order: WNi/HCTY28 > WNi/HTY28 > WNi/HCTY15. Nevertheless, after sulfidation, the BEs decreased in the order: WNi/HTY28 > WNi/HCTY28 ≈ WNi/HCTY15. This means that the interaction between W or Ni and supports or other metal atoms on HCTY was reduced more than that on HTY due to sulfidation. The weaker interaction

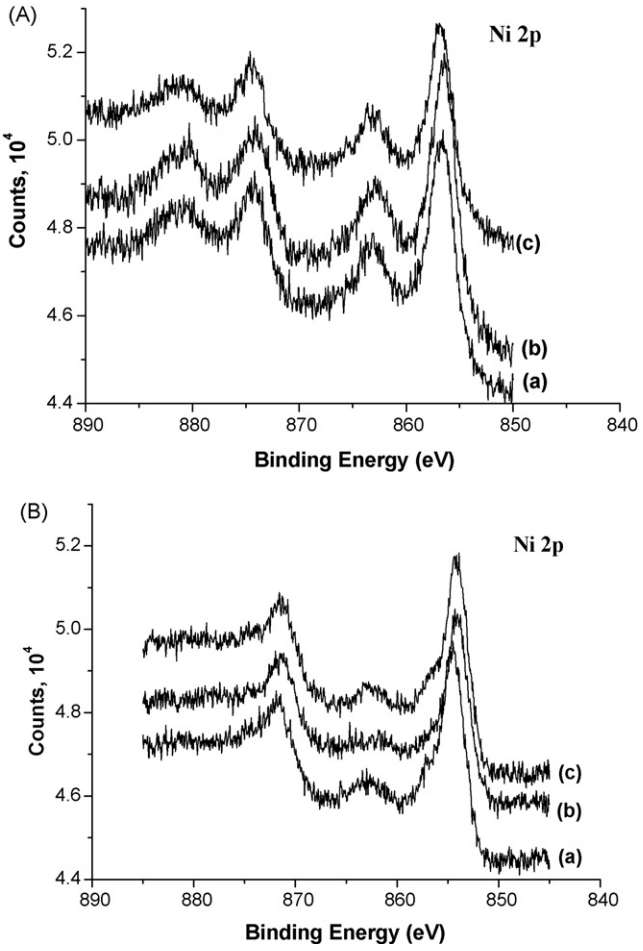

Fig. 6. XPS Ni 2p spectra of oxidic (A) and sulfided (B) catalysts: (a) WNi/HTY28; (b) WNi/HCTY15; (c) WNi/HCTY28.

for WNi/HCTY28 well paralleled the observation from TEM that WNi/HCTY28 had bigger WS_2 crystallines than WNi/HTY28. The lower BEs and the bigger WS_2 crystals are virtually caused by the weaker interaction between the metals and supports.

The sulfidation degree of the catalysts can be predicted by the atomic ratios of S/W + Ni. Theoretically, if the S/W + Ni of the W–Ni catalyst with a W/Ni atomic ratio of 1.29 can be fully sulfided, the S/W + Ni should be equal to 1.42, corresponding to WS_2 and Ni_3S_2 phase formation. The S/W + Ni ratios for all catalysts were higher than the theoretical ratio (1.42), suggesting that very small tungsten and/or nickel sulfide clusters contain more than stoichiometric amount of sulfur [31]. This can also be interpreted as an increase of the sulfidation degree. W and Ni in all catalysts presented a very high degree of sulfidation. Coincidently, the sulfidation degree of the three catalysts followed the same order as BEs, e.g. WNi/HTY28 > WNi/HCTY28 ≈ WNi/HCTY15. Although WNi/HTY28 and WNi/HCTY28 contained the same amount of zeolites (28 wt%), the BEs and sulfidation degree of WNi/HCTY28 were similar to those of WNi/HCTY15, suggesting that the surface properties of zeolites rather than the their content probably controls the interaction between the metal atoms and the supports, and the sulfidation degree.

Table 5
Binding energies, surface W and Ni distribution, and sulfidation degree of oxidic and sulfided W–Ni catalysts

Sample	WNi/HTY28	WNi/HCTY15	WNi/HCTY28
Oxidic			
Bulk W/Ni	1.29	1.29	1.29
Binding energy (eV)			
W $4f_7$	35.81	35.72	36.01
W $4f_5$	37.93	37.86	38.13
Ni $2p_3$	856.57	856.36	856.71
W/Si + Al	0.117	0.088	0.111
Ni/Si + Al	0.065	0.060	0.060
W/Ni	1.80	1.47	1.85
Sulfided			
Binding energy (eV)			
W $4f_7$	32.63	32.48	32.47
W $4f_5$	34.82	34.66	34.66
Ni $2p_3$ (NiS)	854.36	853.90	853.86
Ni $2p_3$ (NiO)	856.90	855.87	856.55
S $2p_3$	162.20	161.98	162.01
W/Si + Al	0.080	0.065	0.087
Ni/Si + Al	0.060	0.044	0.056
W/Ni	1.32	1.48	1.55
S/W + Ni	1.63	1.55	1.57

The surface atomic ratios of Ni/Si + Al and W/Si + Al derived from XPS for each catalyst are given in Table 5. The W/Ni ratios (1.47–1.85) of all oxidic catalysts are higher than that in the bulk (1.29), suggesting that more W species were distributed on the outer surface than they were in the bulk. Compared with WNi/HTY28 and WNi/HCTY28, the W species distributed on the surface of WNi/HCTY15 were much lower. After sulfidation, surface W and Ni species were greatly reduced, indicating that a considerable amount of W and Ni migrated into the bulk. For WNi/HCTY15, W and Ni decreased almost in the same ratio. The W/Ni ratio (1.48) was nearly unchanged. More W than Ni species were decreased on the surfaces of WNi/HTY28 and WNi/HCTY28, which made the W/Ni decrease 26.7% (from 1.80 to 1.32) for WNi/HTY28, and 16.2% (from 1.85 to 1.55) for WNi/HCTY28.

3.5. TEM

The representative TEM images of the three sulfided catalysts are shown in Fig. 7. The TEM images reveal the presence of typical layered structures. In order to find out the species and composition of the layered structure showing in TEM images, EDX analysis was simultaneously carried out on several selected layered areas with TEM. EDX results showed that the species of the layered structure were composed of W and S, and the relative atomic ratio of W and S was 1:2. Therefore, the layered structure was demonstrated to be WS_2. The average number of layers per slab and average slab length were calculated from the measurement of about 300 crystallites. The statistical results of the average length and number of layers of the WS_2 slabs are given in Table 4. For WNi/HCTY15, the average length of WS_2 slabs was 17.7 nm, and the average

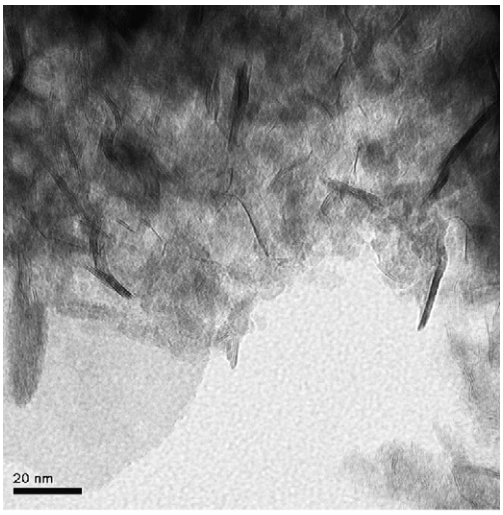

WNi/HTY28

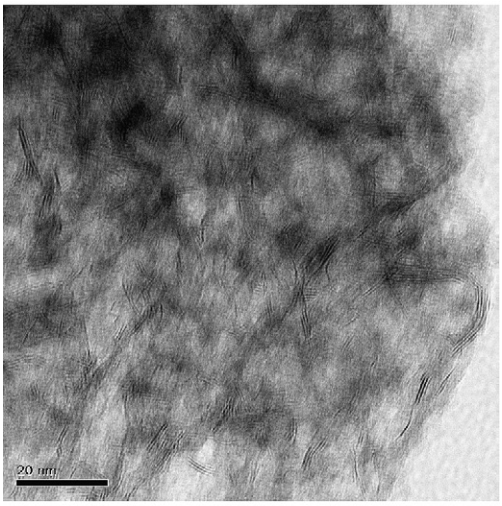

WNi/HCTY15

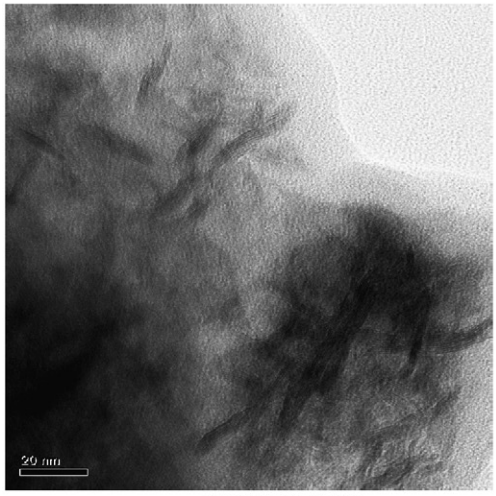

WNi/HCTY28

Fig. 7. TEM images of WNi supported on HTY and HCTY zeolites (the scale bars are 20 nm).

layer number was 4.4. When the zeolite content increased to 28 wt% (WNi/HCTY28), the average slab length increased to 31.9 nm, and the average layer number slightly increased (4.6). However, when the same amount of HTY was added, the average length of WS_2 slabs became 22.4 nm, and the average layer number was almost unchanged (4.7). It has been demonstrated that the size of WS_2 is mostly related to the distribution of WS_2 on the surface of Al_2O_3, irrespective of the type of zeolites [32]. Compared with WNi/HCTY28 and WNi/HTY28, the smaller size of WS_2 on WNi/HCTY15 was produced because of more Al_2O_3 available to distribute on. Probably, less Al_2O_3 was formed on the surface of HCTY zeolite than that on HTY zeolite, owing to the surface silicon enrichment of AHFS treated zeolite [12]. Taking the support as a whole, the quantity of surface Al_2O_3 of WNi/HCTY28 is less than WNi/HTY28. Consequently, larger WS_2 was formed on the surface of WNi/HCTY28 than that of WNi/HTY28.

3.6. Activity evaluation

The LCO hydrotreating results are summarized in Table 6. Fig. 8 shows the relative hydrodenitrogenation (HDN), hydrodesulfurization (HDS), hydrodearomatization (HDA) activities, and <406 K conversion. Fig. 9 presents the saturated, and aromatics hydrocarbon distributions in the final products. LCO used in this experiment, with a high density, high aromatics content, and high sulfur content (Table 1), is a typical inferior feedstock for hydrotreater. HDN activities of the three catalysts were almost identical. More than 99.3 wt% of organic nitrogen compounds was converted. HDS activity decreased in the order: WNi/HTY28 ≈ WNi/HCTY15 > WNi/HCTY28 (Table 5 and Fig. 6), while HDA activity decreased in the order: WNi/HCTY15 ≈ WNi/HCTY28 > WNi/HTY28. Compared with the catalyst containing hydrothermally treated zeolite Y, catalyst containing the chemically treated zeolite Y had much higher activity in HDA, but slightly lower activity in HDS. Therefore, based on feedstocks to be processed and

Table 6
Evaluation in 1 L autoclave with LCO (temperature: 648 K; initial pressure: 8.96 MPa; catalyst/oil weight ratio: 1:10; residence time: 1 h)

	Catalyst		
	WNi/HTY28	WNi/HCTY15	WNi/HCTY28
Nitrogen (ppm)	1.65	1.84	3.43
Sulfur (ppm)	321	355	548
Distillation (K)			
0.5 wt%	388	394	381
5 wt%	421	438	423
10 wt%	444	460	453
30 wt%	493	502	501
50 wt%	526	530	530
70 wt%	469	470	471
90 wt%	637	630	630
99.5 wt%	799	785	779
Liquid yield (wt%)	85.6	88.5	90.9
Cetane index[a]	26.1	27.4	27.4

[a] Calculated based on ASTM D976.

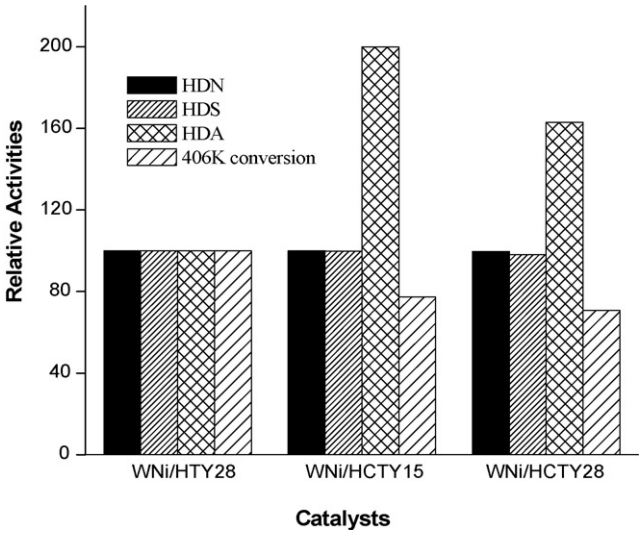

Fig. 8. The relative HDN, HDS, HAD activities, and <406 K conversion.

product requirements, the chemical treatment, hydrothermal treatment, or the combination of both treatments to zeolite Y should be properly chosen to achieve optimal performance in hydrotreating. Apparently, the chemically treated zeolite Y is better in hydroprocessing feeds like LCO than the hydrothermally treated one, due to its higher HDA activity (HDS activity is only slightly lower).

It has been demonstrated that HDS of organic sulfur compounds generally proceeds by two parallel reaction pathways, one by direct desulfurization (DDS) via hydrogenolysis of the C–S bond, and one via hydrogenation of the aromatics ring followed by hydrogenolysis of C–S bond (HYD) [33,34]. The two reaction pathways are believed to take place on the different active sites. Sulfur anion vacancies on the sulfided W and/or Ni are considered to be the active sites for DDS [35], on which the adsorption of sulfur compounds occurs in a predominantly perpendicular configuration. HYD reactions take place on the different sites more likely by a flatwise adsorption [36]. Except for the refractory sulfur species, the HDS of most sulfur compounds preferably proceeds via DDS pathway [37]. Therefore, catalysts with most anion vacancies will exhibit higher activity in HDS. Generally, most vacancies are more readily formed at the edges or corners of sulfided metal slabs on the catalysts. Among the three catalysts, WS_2 slab sizes on WNi/HTY28 and WNi/HCTY15 are smaller than those on WNi/HCTY28. The smaller WS_2 slab can provide more edges and corners as HDS active sites. Thus, WNi/HTY28 and WNi/HCTY15 presented higher HDS activity than WNi/HCTY28. Because the multi-ring aromatics N compounds strongly poisons the hydrogenation path of HDS, but not the DDS path [38], the effect of nitrogen on HDS conversions of the three catalysts seemingly was not pronounced as expected and up to 96 wt% HDS conversion was achieved.

Based on the reaction mechanisms of HDN and aromatics hydrosaturation [39,40], it is generally believed that the hydrogenation of N compounds and aromatics took place on the same site. In contrast to HDS, which may not require complete hydrogenation of the S-ring, in HDN and HDA, the aromatic ring should be saturated before appreciable C–N or C–C cleavage occurs. According to the relative adsorption strength of different compounds on hydroprocessing catalysts was as follows [41]—(a) on acidic sites: N compounds > thiophenic compounds > aromatics; (b) on sulfided active metals: S compounds > N compounds > aromatics. N compounds are more easily and quickly adsorbed on both hydrogenation and acidic sites. Meanwhile, under HDN conditions, aromatics ring saturation is in fact slightly more thermodynamically favoured than N ring saturation, but the N ring is always hydrogenated faster due to kinetic factors [42]. Therefore, on the three catalysts, very high HDN conversion was achieved. Due to the strong inhibition of nitrogen-containing compounds on the hydrogenation reaction of aromatics [43], a low aromatics saturation was obtained on the three catalysts (5.2–10.4%), and the HDA activity decreased in the following order: WNi/HCTY15 > WNi/HCTY28 > WNi/HTY. Under high concentration of N compounds, the higher HDA activity of WNi/HCTY15 and WNi/HCTY28 may be attributed to the good nitrogen-tolerance of HCTY zeolite. According to the Hofmann elimination mechanism of N compounds [44], the Brønsted-acid sites on the catalyst favour the enhancement of HDN reaction. The higher proportion of Brønsted acidic sites in HCTY containing catalysts (Table 2 and Fig. 3) improves the conversion of nitrogen compounds. Faster removal of nitrogen compounds gives aromatics molecules more chance to be adsorbed and converted on the same active sites, and thus a higher HDA activity was obtained.

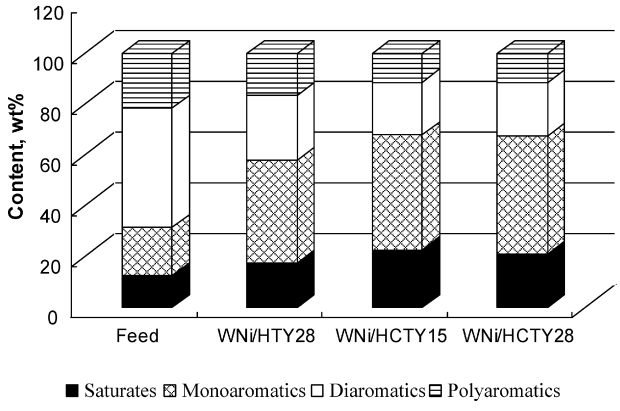

Fig. 9. Saturated and aromatics hydrocarbon distributions on the three catalysts.

As shown in Fig. 9, after hydrogenation, the majority of aromatics were converted to monoaromatics. Monoaromatics are still the compounds with low cetane index. Thus, the cetane index for all catalysts did not greatly increase (in the range of 3.4–4.7). The cetane indexes of WNi/HCTY15 and WNi/HCTY28 were 1.3 units higher than that of WNi/HTY28.

The liquid yield of WNi/HTY28 was 2.9 wt% lower than that of WNi/HCTY15, and 5.3 wt% lower than of WNi/HCTY28. Owing to the long time contact with catalysts in a batch reactor, the paraffin molecules obtained from dealkylation of aromatics and saturates may be over cracked to C1–C4 paraffin molecules which go into gaseous phase and cannot

be recovered. The lower liquid yield of WNi/HTY28 may be associated with its higher acidity.

4. Conclusions

No secondary pores, Lewis acidic sites, and extra-framework aluminum were formed after chemically treating NH_4NaY, while in the hydrothermally treated samples, but considerable amounts of Lewis acidic sites, extra-framework aluminum, and mesopores were produced. Chemically treated zeolite Y has higher "nitrogen-tolerance" than hydrothermal treated zeolite.

After the addition of W and Ni, pore volumes, surface areas, and the acidities were greatly reduced for all three catalysts, while the pore sizes were enlarged. A higher proportion of Brønsted acidity was preserved by chemically treated zeolite Y containing catalysts.

The interaction between W or Ni and support was reduced due to sulfidation. More W species were distributed on the surface than in the bulk. The type of zeolites rather than their content in the catalysts determined the interaction between the metals and the support. The W and Ni distribution on the surface of the catalysts was the same for WNi/HCTY28 and WNi/HTY28. The sizes of WS_2 slabs increased in the order of WNi/HCTY15 > WNi/HTY28 > WNi/HCTY28.

HDN activities of the three catalysts were almost identical. More than 99.3 wt% of organic nitrogen compounds were converted. WNi/HTY28 and WNi/HCTY15 had higher HDS activity than WNi/HCTY28, while WNi/HCTY15 and WNi/HCTY28 had higher HDA activity than WNi/HTY28. The difference in HDN, HDS, and HDA reactivities indicates that the HDS, HDN and HDA reactions occur on the different active sites. Adding zeolite Y with high proportion of Brønsted acidity in the catalysts helped to enhance the hydrodearomatization activity.

References

[1] E. Lecrenay, K. Sakanishi, I. Mochida, Catal. Today 39 (1997) 13–20.
[2] I. Isoda, S. Nagao, X. Ma, Y. Korai, I. Mochida, Energy Fuels 10 (1996) 1078.
[3] C. Song, Catal. Today 86 (2003) 211.
[4] S. Bendezu, R. Cid, J.L.G. Fierro, A.L. Agudo, Appl. Catal. A: Gen. 197 (2000) 47–60.
[5] F. Bataille, J.L. Lemberton, G. Perot, P. Leyrit, T. Cseri, N. Marchal, S. Kasztelan, Appl. Catal. A: Gen. 220 (2001) 191–205.
[6] D. Barthomeuf, J. Phys. Chem. 83 (1979) 249.
[7] B. Beagley, J. Dwyer, F.R. Fitch, R. Mann, J. Walters, J. Phys. Chem. 88 (1984) 1744.
[8] G.T. Kerr, J. Phys. Chem. 71 (1967) 4155.
[9] J. Kinowski, C.A. Fyfe, G.C. Gobbi, J. Chem. Soc. Farad. Trans. I 81 (1985) 3003.
[10] K. Beyer, H.I. Belenykaja, Stud. Surf. Sci. Catal. 5 (1980) 203.
[11] Q.L. Wang, G. Giannetto, M. Guisnet, Zeolites 10 (1990) 301–303.
[12] J.M. Cruz, A. Corma, V. Fornes, Appl. Catal. A: Gen. 50 (1989) 287–293.
[13] W. Breck, D.H. Blass, G.W. Skeels, Union Carbide Corp., US Patent 4,503,023 (1985).
[14] L. Bertea, H.W. Kouwenhoven, R. Prins, Appl. Catal. A: Gen. 129 (1995) 229.
[15] A. Zukal, V. Patzelova, U. Lohse, Zeolites 6 (1986) 133–136.
[16] G. Garralon, A. Corma, V. Fornes, Zeolites 9 (1989) 84–86.
[17] C. Mirodatos, D. Barthomeuf, J. Chem. Soc., Chem. Commun. (1981) 39.
[18] R.J. Pellet, C.S. Blackwell, J.A. Rabo, J. Catal. 114 (1988) 71–89.
[19] B.A. Williams, J.T. Miller, R.Q. Snurr, H.H. Kung, Micropor. Mesopor. Mater. 35–36 (2000) 61–74.
[20] A.I. Biaglow, D.J. Parrillo, G.T. Kokotailo, R.J. Gorte, J. Catal. 148 (1994) 213–223.
[21] P.V. Shertukde, W.K. Hall, J.-M. Dereppe, G. Marcelin, J. Catal. 139 (1993) 468–481.
[22] D. Solis, T. Klimova, R. Cuevas, J. Ramirez, A. Lopez-Agudo, Catal. Today 98 (2004) 201–206.
[23] N. Kunisada, K.-H. Choi, Y. Korai, I. Mochida, K. Nakano, Appl. Catal. A: Gen. 276 (2004) 51–59.
[24] M.A. Ali, T. Tatsumi, T. Masuda, Appl. Catal. A: Gen. 233 (2002) 77–90.
[25] D.W. Breck, Zeolites Molecular Sieves, Wiley, New York, 1974, p. 94.
[26] L. Salvati, J.L. Makovsky, J.M. Stencel, F.R. Brown, D.M. Hercules, J. Phys. Chem. 85 (1981) 3700.
[27] D. Li, A. Nishishjima, D.E. Morris, G.D. Guthrie, J. Catal. 188 (1999) 111–124.
[28] S. Bendezu, R. Cid, J.L.G. Firro, A.L. Agudo, Appl. Catal. A: Gen. 197 (2000) 47–60.
[29] B. Pawelec, L. Daza, J.L.G. Fierro, J.A. Anderson, Appl. Catal. A 145 (1996) 307.
[30] L. Portela, P. Grange, B. Delmon, J. Catal. 156 (1995) 243.
[31] Y.W. Li, X.Y. Pang, B. Delmon, J. Mol. Catal. A: Chem. 169 (2001) 259.
[32] L. Ding, Y. Zheng, Z. Zhang, Z. Ring, J. Chen, in preparation.
[33] M.L. Vrinat, Appl. Catal. 6 (1983) 137.
[34] M. Houalla, N.K. Nag, A.V. Sapre, D.H. Broderick, B.C. Gates, AIChE J. 24 (1978) 1015.
[35] F. Ruette, E.V. Ludena, J. Catal. 67 (1981) 266.
[36] P. Desikan, C. Amberg, Can. J. Chem. 42 (1964) 843.
[37] R. Shafi, G.J. Hutchings, Catal. Today 59 (2000) 423–442.
[38] M. Nagai, T. Kabe, J. Catal. 81 (1983) 440.
[39] L. Ding, Z. Zhang, Y. Zheng, Z. Ring, J. Chen, Appl. Catal. A 301 (2006) 241.
[40] M.V. Bhinde, S. Shih, R. Zawadski, J. Katzer, H. Kwart, in: H.F. Barry, P.C.H. Mitchell (Eds.), Proceedings of the 3rd International Conference on Chemistry and Uses of Molybdenum, Climax Molybdenum Company, (1979), p. 184.
[41] J.N. Beltramini, T.J. Wessel, R. Datta, in: B. Delmon, G.F. Fromet (Eds.), Catalyst Deactivation, Elsevier, Amsterdam, 1991, p. 119.
[42] E.W. Stern, J. Catal. 57 (1979) 390.
[43] P.S. Ting, C.W. Curtis, D.C. Cronauer, Energy Fuel 6 (1992) 511.
[44] N. Nelson, R.B. Levy, J. Catal. 58 (1979) 485.